

From a superconductor NdNiO₂ to a Mott multiferroic BiNiO₂

Hu Zhang*, RuiFeng Zhang, Lulu Zhao, Chendong Jin, Ruqian Lian, Peng-Lai Gong,

RuiNing Wang, JiangLong Wang, and Xing-Qiang Shi

Key Laboratory of Optic-Electronic Information and Materials of Hebei Province,

Research Center for Computational Physics, College of Physics Science and

Technology, Hebei University, Baoding 071002, P. R. China

* E-mails: zhanghu@hbu.edu.cn

Motivated by the recently discovered superconductivity in Sr-doped nickelate oxides NdNiO₂, we predict a material BiNiO₂ that provides an opportunity to study the intertwined ferroelectricity, metallicity, and magnetism in a crystal with very simple atomic structures. There is a ferroelectric structural transition from the nonpolar phase with the $P4/mmm$ space group to the polar phase with the $P4mm$ space group, which is driven by the lone pair on Bi. Calculations based on the Heyd-Scuseria-Ernzerhof hybrid density functional reveal that both the nonmagnetic and ferromagnetic states are metallic for nonpolar and polar phases, while the lowest energy ground-state for polar BiNiO₂ is a Hubbard Mott insulator with the G-type antiferromagnetic spin configurations. As a ferroelectric material with an electric polarization of 0.49 C/m², it may be possible to control the magnetic order in BiNiO₂ by an applied electric field. The replacement of Nd by Bi serves as a connecting link between a high-temperature superconductor and a Mott multiferroic. Our work supports a route towards strongly correlated ferroelectrics.

I. INTRODUCTION

There are two important types of coupled physical properties in ferroelectrics. One is the interplay between the ferroelectricity and magnetism [1]. Such materials are usually called multiferroics. The coexistence of ferroelectric and magnetic order in multiferroics provides a route for the control of magnetism by applications of an electric field. This magnetoelectric coupling makes these materials be useful for

technological applications including sensors, spintronics, multifunctional memory, and so on. BiFeO_3 is one of the typical multiferroics having magnetic and ferroelectric order at room temperature [1]. The other of the two types of coupled physical properties in ferroelectrics is the interplay between the ferroelectricity and metallicity. At first sight it seems that metallic materials cannot exhibit ferroelectricity because conduction electrons will screen internal electric fields [2]. In 1965, Anderson and Blount predicted the possibility of a “ferroelectric metal” [3]. In other words, there was a ferroelectric-like structural transition in the metallic material. In 2013, a ferroelectric-like structural transition in the metallic LiOsO_3 was discovered experimentally [4]. Such materials are also called polar metals due to its ferroelectric-like polar crystal structures. Other works on polar metals have also been published [5-7]. Elemental polar metals (group V elements crystallize in the $P6_3mc$ space group) were also predicted [8]. From a fundamental standpoint, the coupling of disparate physical properties including ferroelectricity, metallicity, and magnetism in a single phase is very interesting.

In this work, we theoretically predict a material BiNiO_2 which allows us to study the intertwined ferroelectricity, metallicity, and magnetism, as shown in Fig. 1, in a crystal with very simple atomic structures. This prediction is partly motivated by the recently discovered superconductivity in Sr-doped nickelate oxides NdNiO_2 having the $P4/mmm$ (No. 123) space group [9]. In experiments, the infinite layered phase NdNiO_2 was obtained from the reduced form of perovskite nickelates NdNiO_3 . Similar to NdNiO_2 , we may expect that BiNiO_2 can be synthesized experimentally from the reduced form of perovskite nickelates BiNiO_3 . Our results indicate that there are one unstable polar-mode (imaginary frequencies of phonons) in BiNiO_2 with the $P4/mmm$ symmetry due to the lone pair on Bi. According to the soft-mode theory of ferroelectrics, this unstable phonon drives a ferroelectric structural transition, in which nonpolar BiNiO_2 transforms into a polar state with the $P4mm$ (No. 99) space group without the inversion symmetry. Similar to NdNiO_2 , BiNiO_2 has the strongly correlated electronic structures. We find that both the nonmagnetic and ferromagnetic

states of the nonpolar and polar BiNiO₂ are all metallic. The G-type antiferromagnetic (AFM between NiO₂ planes along the c direction and AFM within the NiO₂ plane) state has the lowest ground-state energy for polar BiNiO₂. In fact, the polar phase of BiNiO₂ is a Mott insulator. Therefore, the ferroelectric state of BiNiO₂ provides a good platform to study various coupled physical properties.

II. METHODOLOGY

We have performed first-principles calculations based on density functional theory (DFT) [10] with the local density approximation (LDA) and Perdew–Burke–Ernzerhoff (PBE) functional in generalized gradient approximation (GGA) [11] in the Vienna Ab Initio Simulation Package (VASP) [12-14]. The Heyd-Scuseria-Ernzerhof (HSE) hybrid functional [15] was used to obtain the strongly correlated electronic structures. We used a $12 \times 12 \times 12$ Monkhorst-Pack grid [16] in the LDA and PBE calculations with an energy cutoff of 500 eV. For HSE calculations, a $6 \times 6 \times 6$ Monkhorst-Pack grid was used. The crystal structures were relaxed until the Hellmann-Feynman forces are less than 1 meV/Å. The Berry phase method [17] was used to calculate the electric polarization. The phonon spectra were calculated with phonopy [18]. The tight-binding models were constructed with the maximally localized Wannier functions using Wannier90 package [19,20]. The $k \cdot p$ method was used to obtain the effective Hamiltonian describing the quadratic band-crossing point (QBCP).

III. RESULTS AND DISCUSSION

A. The ferroelectric structural transition

According to experimental results, NdNiO₂ has the $P4/mmm$ space group with the lattice constants $a = 3.9208$ Å, $c = 3.281$ Å. Nd, Ni, O1, and O2 atoms site at the $1d$ ($1/2, 1/2, 1/2$), $1a$ ($0, 0, 0$), and $2f$ ($0, 1/2, 0$) ($1/2, 0, 0$) Wyckoff positions respectively [21]. These crystal structure parameters are used as the initial input for the nonpolar BiNiO₂ and then we relax them fully. For the LDA calculations we obtain $a = 3.835$ Å,

$c = 3.324 \text{ \AA}$. While PBE gives $a = 3.931 \text{ \AA}$, $c = 3.395 \text{ \AA}$. It is well known that LDA and PBE usually underestimate and overestimate the lattice constants slightly, respectively, compared to the experimental values. The calculated structural parameters for nonpolar BiNiO_2 are collected in Table I. Our calculation results indicate that BiNiO_2 and NdNiO_2 have similar lattice constants. We find that the LDA and PBE crystal structure parameters give nearly identical electronic structures. Hence, we will use the crystal structure parameters obtained with LDA calculations in the following. The atomic structures of nonpolar BiNiO_2 are shown in Fig. 2(a), in which four O atoms surround the Ni in a planar square environment.

According to the soft-mode theory of ferroelectrics, there exist unstable polar phonons in the nonpolar high-symmetry reference structure in first-principles calculations [1]. From the factor group analysis, the nonpolar BiNiO_2 with $P4/mmm$ symmetry has 3 acoustic modes and 9 optical modes at the Brillouin zone center. Optical modes can be expressed as

$$3E_u + B_{2u} + 2A_{2u}, \quad (1)$$

where the three two-fold degeneracy E_u modes and two A_{2u} modes are infrared active. The calculated frequencies of modes at the Brillouin zone center are given in Table II. We find one unstable polar-mode with an imaginary frequency of 215 cm^{-1} (denoted as a negative value). This is one of the A_{2u} modes, in which Ni and O sublattices move against each other along the c direction and Bi not at rest. This phonon mode is polarized along the c direction with the calculated displacement eigenvector of $[\delta(\text{Bi}) = -0.190, \delta(\text{Ni}) = -0.325, \delta(\text{O}) = +0.655]$. It is this unstable phonon that drives a ferroelectric structural transition from the nonpolar state to the polar state. To further study the dynamic stabilities of the nonpolar state BiNiO_2 , we have also calculated the phonon spectra in the entire Brillouin zone. The dispersion curves along high symmetry directions are plotted in Fig. 3(a). The nonpolar phase also exhibits imaginary phonon frequencies at the $A(0.5, 0.5, 0.5)$ point. Thus, the $P4/mmm$ BiNiO_2 is dynamically unstable that is the same as the nonpolar high-symmetry reference state of other typical ferroelectrics such as BaTiO_3 .

By freezing the phonon with an imaginary frequency at the Brillouin zone center, it is possible to convert the nonpolar state into a dynamically stable polar state. We add displacements to atoms in the nonpolar state BiNiO₂ according to the calculated displacement eigenvector. Then the new structure is fully relaxed. The LDA calculations give $a = 3.787 \text{ \AA}$, $c = 3.544 \text{ \AA}$. Bi, Ni, O1, and O2 atoms site at the $1b$ (1/2, 1/2, 0.5709), $1a$ (0, 0, 0.0482), and $2c$ (0, 1/2, 0.9554) (1/2, 0, 0.9554) Wyckoff positions respectively. While PBE gives optimized structural parameters of $a = 3.893 \text{ \AA}$, $c = 3.702 \text{ \AA}$ with Bi, Ni, O1, and O2 atoms locating at the $1b$ (1/2, 1/2, 0.5938), $1a$ (0, 0, 0.0392), and $2c$ (0, 1/2, 0.9484) (1/2, 0, 0.9484) Wyckoff positions respectively. The calculated structural parameters of polar BiNiO₂ are collected in Table I. The resulting state is a polar phase with the polar space group $P4mm$. In Fig. 2(b) we show the atomic structures of the polar BiNiO₂. The relative displacements along the c direction between Ni and O are clear.

The polar BiNiO₂ with $P4mm$ symmetry has 3 acoustic modes and 9 optical modes at the Brillouin zone center. Optical modes can be expressed as

$$3E + B_1 + 2A_1, \quad (2)$$

where the three two-fold degeneracy E modes and two A_1 modes are both infrared and Raman active, while one B_1 mode is Raman active. The calculated frequencies of modes at the Brillouin zone center are given in Table II. There are no modes with imaginary frequencies. The phonon spectra of polar BiNiO₂ are shown in Fig. 3(b). Obviously, there are no imaginary phonon frequencies through the entire Brillouin zone, which indicates the dynamic stabilities of the polar state BiNiO₂. The energy difference between the nonpolar and polar states is 0.13 eV and 0.19 eV for LDA and PBE calculations respectively, which are comparable to typical ferroelectrics (0.2 eV for PbTiO₃). This suggests the possibility of realistic switching of polarizations in BiNiO₂. The soft phonon mode A_{2u} in the nonpolar state is energetically favorable to drive a ferroelectric structural transition from the nonpolar high-symmetry state with the $P4/mmm$ symmetry into a polar $P4mm$ state. We conclude that $P4mm$ BiNiO₂ is a ferroelectric material with the $P4/mmm$ state as its high symmetry paraelectric state.

This is a new type of crystal structure exhibiting ferroelectricity, which can be called the $P4mm$ BiNiO₂ structure type.

B. Electronic structures of nonmagnetic states

According to the previous study on strongly correlated NdNiO₂ and perovskite nickelates RNiO₃ (R is Bi or a rare-earth metal), the HSE hybrid functional method was essential to obtain reliable theoretical results which are consistent with experimental data [22]. Hence, we use the HSE hybrid functional to calculate electronic structures of BiNiO₂. In Fig. 4(a) and Fig. 5(a) we show the HSE06 band structures of nonpolar and polar BiNiO₂ in the nonmagnetic state. For the nonpolar BiNiO₂, the O 2*p* bands distribute from -10 to -5 eV, while the Ni 3*d* bands extend from -5 to 2.5 eV. The Ni 3*d*_{*x*²-*y*²} crosses the Fermi energy. Around the M point, Bi 6*p*_{*x/y*} states form electron pockets. There is strong mixing between Ni 3*d*_{*x*²-*y*²} orbital and Bi 6*p*_{*x/y*} orbitals along the X-M- Γ direction. At the M point, the Ni 3*d*_{*x*²-*y*²} state is located at just below the Bi 6*p*_{*z*} state. The Bi 6*p*_{*z*} state goes down along the Γ -Z direction and up along the Z-R direction, forming an electron pocket around Z. In NdNiO₂, the Ni 3*d*_{*x*²-*y*²} and Nd 5*d*_{*z*²} states cross the Fermi energy. Compared to NdNiO₂, Bi 6*p*_{*x/y*} states change dispersions of the Ni 3*d*_{*x*²-*y*²} state notably [22,23]. The Ni 3*d*_{*x*²-*y*²}, 3*d*_{*xz/yz*} and 3*d*_{*xy*} bands have weak dispersions along the Γ -Z direction, which show two-dimensional features. The Ni 3*d*_{*z*²} state lies above the 3*d*_{*xy*} state different from the case in NdNiO₂. The Ni 3*d*_{*z*²} state in NdNiO₂ is more dispersive along the Γ -Z direction than that in BiNiO₂. As shown in Fig. 5(a), the nonmagnetic state of polar BiNiO₂ is also metallic. The band structures around the Fermi energy can be compared with those in the nonpolar BiNiO₂. The electron pockets formed by Bi 6*p*_{*x/y*} and 6*p*_{*z*} states are raised in energy. The states at the Fermi energy are reduced for the structural transition from the nonpolar state to the polar state. Compared to nonpolar BiNiO₂, the Ni 3*d* bands in polar BiNiO₂ are

flatter.

To further understand electronic structures of nonpolar and polar BiNiO₂, we obtain on-site energies and hoppings parameters from the Wannier fitting of 14 bands around the Fermi energy corresponding to mainly Bi *p* (3 states), Ni *d* (5 states), and O *p* (2×3 states) in the HSE06 calculations. The results are given in Table III. The amplitudes of hop between Ni *d* and O *p* orbitals for nonpolar BiNiO₂ are larger than these of polar BiNiO₂. The amplitudes of hop among O $2p_{x/y}$ orbitals are nearly identical for two phases. There is also significant hybridization between Ni *d* and Bi *p* orbitals. The Wannier functions are shown in Fig. 4(b) and Fig. 5(b) for nonpolar and polar BiNiO₂ respectively. They give *d*-like orbitals centered on Ni and *p*-like on the O and Bi sites. For the $3d_{x^2-y^2}$ orbitals, there are some O $2p$ contributions.

The electron density of polar BiNiO₂ in the (2 0 0) plane is plotted in Fig. 6(a). A highly asymmetric electron density distribution on Bi can be found, which looks like an asymmetric lobe. As shown in Fig. 6(b), the main peak of Bi 6*s* states locate at around -14 eV. There are also lots of states distribute from -10 to -2 eV, where O $2p$ bands also lie at. Thus, the “core” Bi 6*s* states hybridize with O $2p$ sates forming the asymmetric lobe. This is the typical mechanism of the lone pair driven ferroelectric structure transition [24]. Above results suggest that Bi not only drives the structural transition but also changes the electronic structures around the Fermi energy.

C. Electronic structures of magnetic states

We now consider the ferromagnetic states. The energy difference between the nonmagnetic state and the ferromagnetic state of nonpolar BiNiO₂ is 0.54 eV calculated with the HSE06 functional. The local moment of Ni 3*d* is 0.90 μ_B, similar to that in NdNiO₂ (0.94 μ_B). In Fig. 7 we plot band structures of the ferromagnetic state for nonpolar BiNiO₂. There is a large splitting between the spin minority and majority channels of the Ni $3d_{x^2-y^2}$ orbital (about 6 eV). For the spin minority channel, the Bi 6*p* states are separated with occupied Ni 3*d* sates forming an energy

gap at each k points. For polar BiNiO₂, the energy difference between the nonmagnetic state and the ferromagnetic state is 0.60 eV. The local moment of Ni 3d is 0.93 μ_B . The ferromagnetic state of polar BiNiO₂ is metallic as shown in Fig. 8. This is a state in which the ferroelectricity, metallicity and magnetism coexist. The splitting between the spin minority and majority channels of the Ni 3d_{x²-y²} orbital is about 5 eV. Compared to nonpolar BiNiO₂, states around the Fermi energy are significantly reduced as the result of the raising of Bi 6p states in two spin channels and reducing of the Ni 3d_{x²-y²} state in the spin majority channel. For both the nonmagnetic state and the ferromagnetic state, the ferroelectric structural transition in BiNiO₂ always follows reducing of states at the Fermi energy, indicating the competition between ferroelectricity and metallicity.

For the spin majority channel of the polar BiNiO₂, occupied and unoccupied sates are only connected at the M point forming a QBCP just below the Fermi energy contributed from Bi 6p_{x/y} states, as can be found in Fig. 8(a). The site symmetry of the M point is C_{4v}, which has only one two-dimensional irreducible representation E allowing the existence of QBCP [25,26]. The point group C_{4v} consists of two generators including a fourfold rotation c_{4z} ($-y, x, z$) around the z axis and a mirror symmetry σ_{v1} ($-x, y, z$). The representations of group generators for the two-dimensional irreducible representation E are given by

$$\begin{aligned} D(c_{4z}) &= \begin{pmatrix} 0 & -1 \\ 1 & 0 \end{pmatrix}, \\ D(\sigma_{v1}) &= \begin{pmatrix} 0 & -1 \\ -1 & 0 \end{pmatrix}. \end{aligned} \quad (3)$$

The theory of invariant gives the following constraint on $k \cdot p$ model

$$D(R)H(k)D^\dagger(R) = H(R(k)), \quad (4)$$

where $D(R)$ is the representative matrix of operator R . Based on these we obtain the $k \cdot p$ effective Hamiltonian describing the QBCP

$$H(k) = \alpha_1(k_x^2 + k_y^2)\sigma_0 + \alpha_2(k_x^2 - k_y^2)\sigma_x + \alpha_3(k_x k_y)\sigma_z, \quad (5)$$

where $k_{x,y}$ are wave vectors related to the QBCP, $\sigma_{x,z}$ are the Pauli matrices

denoting orbitals not spin, σ_0 is the 2×2 identity matrix, $\alpha_{1,2,3}$ are material-dependent real parameters, and the energy of the QBCP is set to zero for simplicity, which corresponds to that the Fermi energy of polar BiNiO₂ is turned to its QBCP. The eigenvalues are

$$E(k) = \alpha_1(k_x^2 + k_y^2) \pm \sqrt{\alpha_2^2(k_x^2 - k_y^2)^2 + \alpha_3^2 k_x^2 k_y^2}. \quad (6)$$

The quadratic band-crossing character can be understood from these eigenvalues. The QBCP in the spin majority channel of polar BiNiO₂ is protected by C_4 rotational symmetry.

Like NdNiO₂, the G-type AFM state displayed in Fig. 9(a) is found to be the lowest energy ground-state for polar BiNiO₂ [22]. The electronic structures are studied by setting the G-type AFM spin configurations on Ni using a $\sqrt{2} \times \sqrt{2} \times 2$ supercell. The HSE06 hybrid functional bands are plotted in Fig. 9(b). Due to the strong correlation in BiNiO₂, the Ni $3d_{x^2-y^2}$ bands split into lower and upper Hubbard bands separated by about 6 eV due to the AFM spin configuration. The lower Hubbard Ni $3d_{x^2-y^2}$ band is located higher than the Ni $3d_{z^2}$ band different from the case in NdNiO₂ where the lower Hubbard Ni $3d_{x^2-y^2}$ band is located below the Ni $3d_{z^2}$ band. This suggests different influences of Bi and Nd on the NiO₂ plane. Bi changes both the atomic and electronic structures of the NiO₂ plane. At the Γ point, the Bi $6p_z$ state forms the conduction band minimum and the Bi $6p_{x/y}$ states are just located at above it. HSE06 results indicate that the polar BiNiO₂ is a Hubbard Mott insulator. On the other hand, the computed electric polarization of polar BiNiO₂ is 0.49 C/m², which is comparable with typical ferroelectrics. The electric polarization in ferroelectrics can be switched by an applied electric field. Hence, as a multiferroic material, it may be possible to control the magnetic order in BiNiO₂ by an applied electric field experimentally, which can be studied detailly in future works.

IV. CONCLUSIONS

In summary, we have predicted a material BiNiO_2 which undergoes a ferroelectric structure transition from the nonpolar $P4/mmm$ phase to the polar $P4mm$ phase. Both the nonmagnetic and ferromagnetic states are metallic for nonpolar and polar BiNiO_2 . A rotational symmetry protected QBCP is found for the spin majority channel of the polar BiNiO_2 in the ferromagnetic state. The lowest energy ground-state for polar BiNiO_2 is a Hubbard Mott insulator with the G-type AFM spin configurations on Ni. The predicted material BiNiO_2 provides a good platform to study various coupled physical properties including ferroelectricity, metallicity, and magnetism. Through the substitution of Nd by Bi, we transform the high-temperature superconductor NdNiO_2 to a strongly correlated ferroelectric material BiNiO_2 . This method may be used to design other interesting multifunctional materials based on known high-temperature superconductors.

ACKNOWLEDGMENTS

This work was supported by the Advanced Talents Incubation Program of the Hebei University (Grants No. 521000981423, No. 521000981394, No. 521000981395, and No. 521000981390), the Natural Science Foundation of Hebei Province of China (Grants No. A2021201001 and No. A2021201008), the National Natural Science Foundation of China (Grants No. 12104124 and No. 12274111), and the high-performance computing center of Hebei University.

TABLE I. The lattice constants and atomic positions of nonpolar and polar states of BiNiO₂ calculated with LDA.

Structural parameters	Nonpolar	Polar
a	3.835 Å	3.787 Å
c	3.324 Å	3.544 Å
Bi	$1d$ (1/2,1/2,1/2)	$1b$ (1/2,1/2,0.5709)
Ni	$1a$ (0,0,0)	$1a$ (0,0,0.0482)
O1	$2f$ (0,1/2,0)	$2c$ (0,1/2,0.9554)
O2	(1/2,0,0)	(1/2,0,0.9554)

TABLE II. The frequencies of the zone-center phonon modes in nonpolar and polar states of BiNiO₂. The imaginary frequency is denoted as a negative value.

Nonpolar		Polar	
Model	Frequency (cm ⁻¹)	Model	Frequency (cm ⁻¹)
E _u	546	E	530
E _u	205	E	366
B _{2u}	121	B ₁	320
A _{2u}	49	A ₁	319
E _u	20	A ₁	134
A _{2u}	-215	E	110

TABLE III. Calculated Wannier on-site energies and hoppings for nonpolar and polar states of BiNiO₂ in the HSE06 simulations. O1 bonds to Ni along the y direction, and O2 bonds to Ni along the x direction.

Wannier on-site energies (eV)	Nonpolar	Polar
d_{z^2}	-2.93	-3.06
$d_{xz/yz}$	-3.43	-3.45
$d_{x^2-y^2}$	-0.95	-1.09
d_{xy}	-3.97	-4.09
p_z O1	-5.45	-5.60
p_x O1	-5.25	-5.01
p_y O1	-6.57	-6.63
p_z O2	-5.45	-5.60
p_x O2	-6.57	-6.63
p_y O2	-5.25	-5.01
p_z Bi	1.58	1.11
p_x Bi	0.74	0.72
p_y Bi	0.74	0.72
Wannier hoppings (eV)		
$d_{xy} - p_y$ O2	-0.83	-0.79
$d_{xz} - p_z$ O2	-0.91	-0.77
$d_{x^2-y^2} - p_x$ O2	1.74	1.63
$d_{z^2} - p_x$ O2	-0.59	-0.48
p_y O2 - p_x O1	0.18	0.14
p_x O2 - p_x O1	0.34	0.32
p_y O2 - p_y O1	0.34	0.32
p_x O2 - p_y O1	-0.69	-0.70
p_z O2 - p_z O1	0.13	0.09
$d_{z^2} - p_z$ Bi	0.10	0.17
$d_{z^2} - p_x$ Bi	0.30	0.27
$d_{xz} - p_x$ Bi	0.21	0.23
$d_{xy} - p_x$ Bi	0.13	0.10

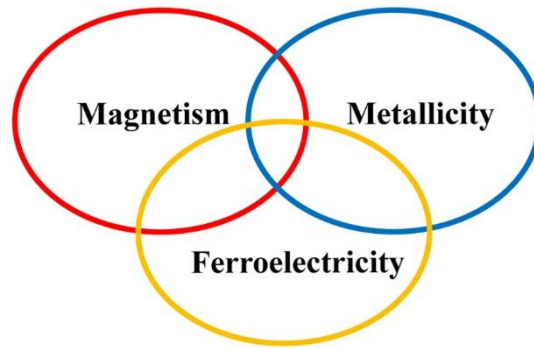


FIG. 1. The schematic plot of intertwined ferroelectricity, metallicity, and magnetism in materials.

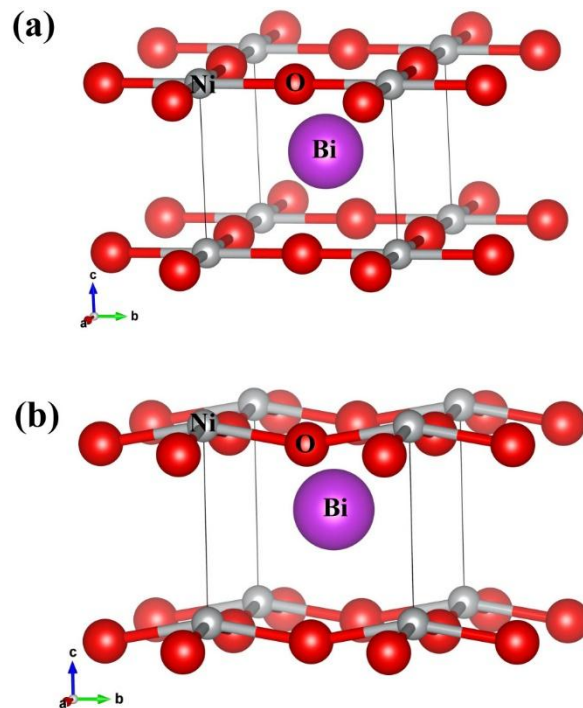


FIG. 2. The crystal structures of (a) the nonpolar BiNiO₂ with the $P4/mmm$ symmetry (No. 123) and (b) the polar BiNiO₂ with the $P4mm$ symmetry (No. 99).

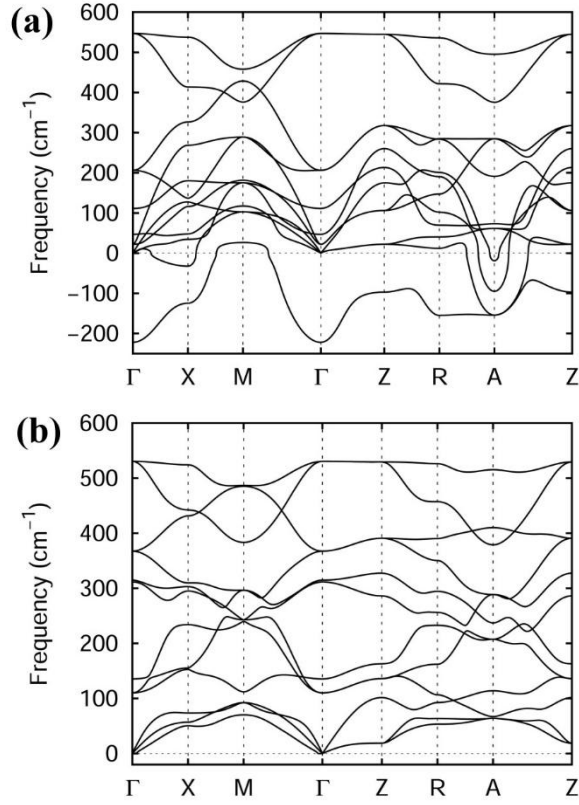


FIG. 3. Phonon spectrum of (a) the nonpolar and (b) the polar BiNiO₂ along the $\Gamma(0, 0, 0)$ -X(0, 0.5, 0)-M(0.5, 0.5, 0)- Γ -Z(0, 0, 0.5)-R(0, 0.5, 0.5)-A(0.5, 0.5, 0.5)-Z directions. The imaginary frequencies are indicated as negative values.

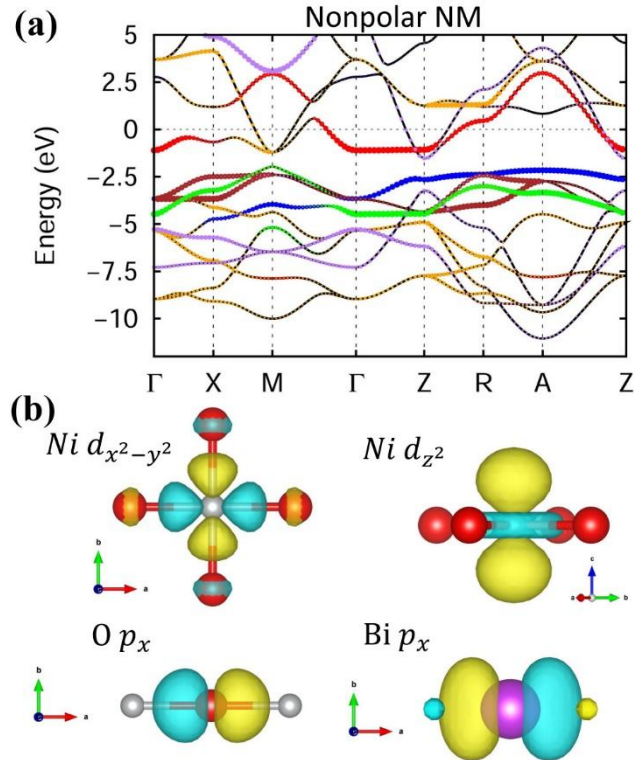


FIG. 4. (a) HSE06 band structures of the nonmagnetic state in the nonpolar BiNiO₂ along the $\Gamma(0, 0, 0)$ -X(0, 0.5, 0)-M(0.5, 0.5, 0)- Γ -Z(0, 0, 0.5)-R(0, 0.5, 0.5)-A(0.5, 0.5, 0.5)-Z directions. The projected band structures of d orbitals (red for $d_{x^2-y^2}$, blue for d_{z^2} , brown for $d_{xz/yz}$, and green for d_{xy}) in Ni and $2p$ orbitals (orange for $p_{x/y}$ and purple for p_z) in Bi and O are also shown. The Fermi level is set at zero eV. (b) Wannier functions of the $d_{x^2-y^2}$, d_{z^2} and p_x character for nonpolar BiNiO₂. The sign of the Wannier function is represented by colors.

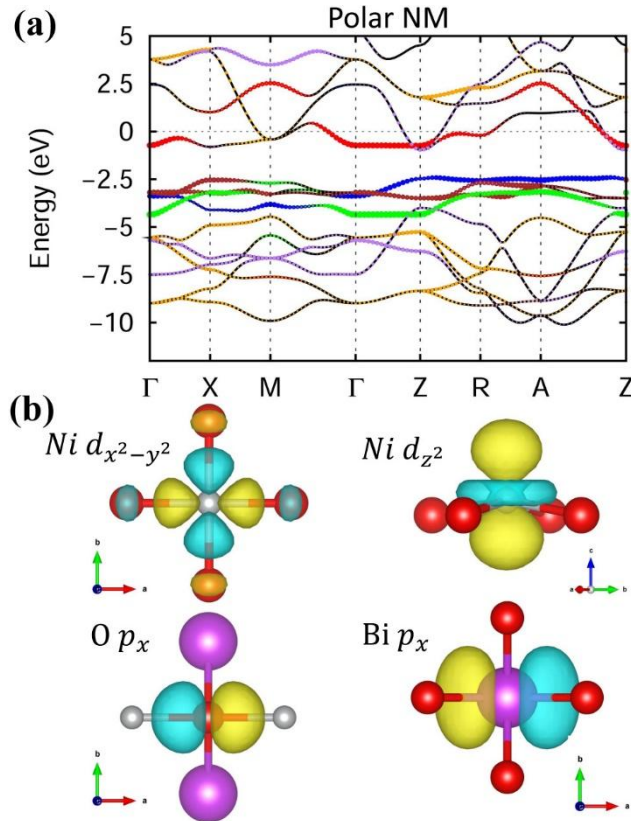


FIG. 5. (a) HSE06 band structures of the nonmagnetic state in the polar BiNiO₂. (b) Wannier functions of the $d_{x^2-y^2}$, d_{z^2} and p_x character for polar BiNiO₂. The sign of the Wannier function is represented by colors. The color in band structures has the same meanings as in Fig. 4.

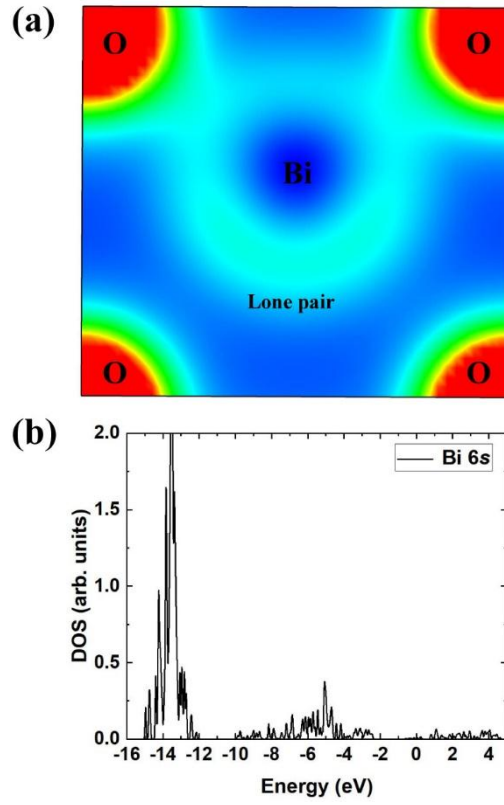


FIG. 6. (a) Electron densities and (b) partial (Bi 6s orbitals) density of states for polar BiNiO₂.

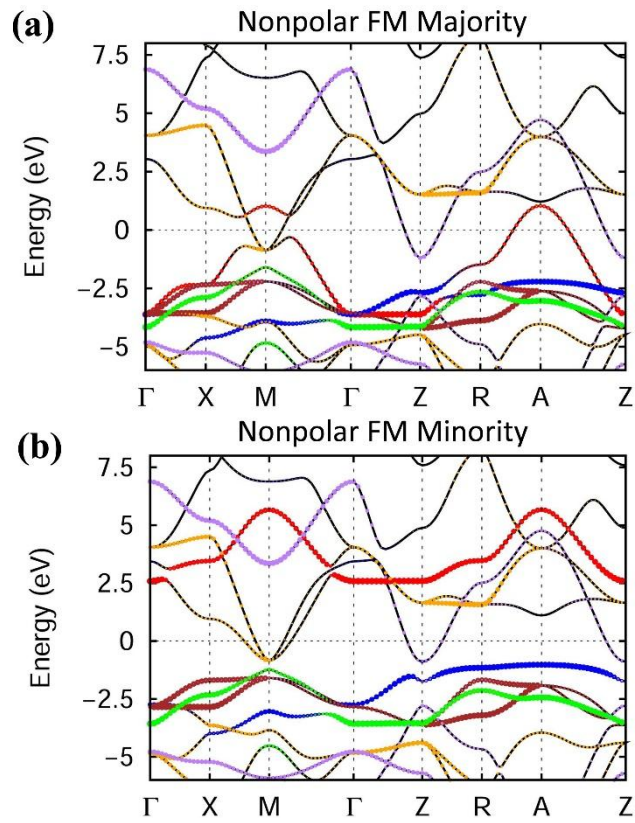


FIG. 7. HSE06 band structures of the ferromagnetic state of the spin (a) majority (b) minority

channels in the nonpolar BiNiO₂. The color has the same meanings as in Fig. 4.

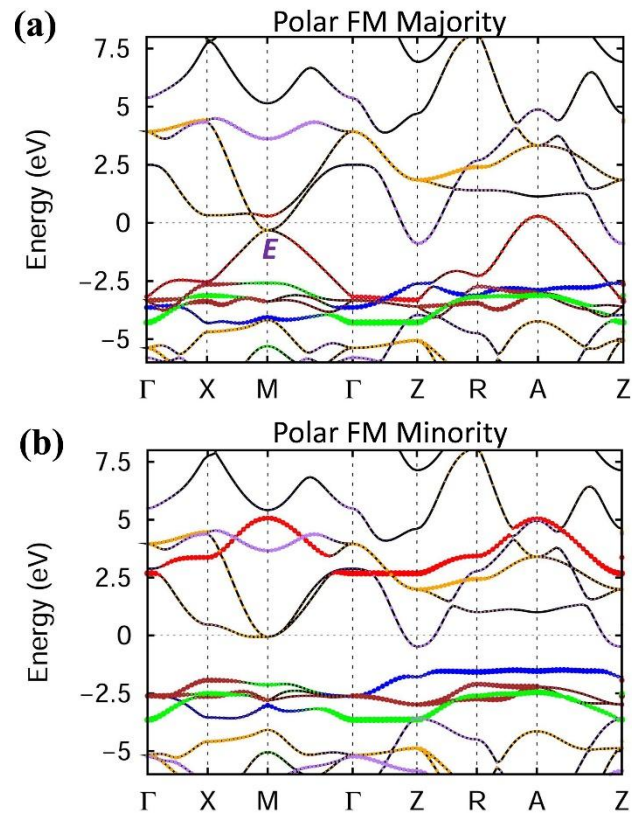


FIG. 8. HSE06 band structures of the ferromagnetic state of the spin (a) majority (b) minority channels in the polar BiNiO₂. The color has the same meanings as in Fig. 4.

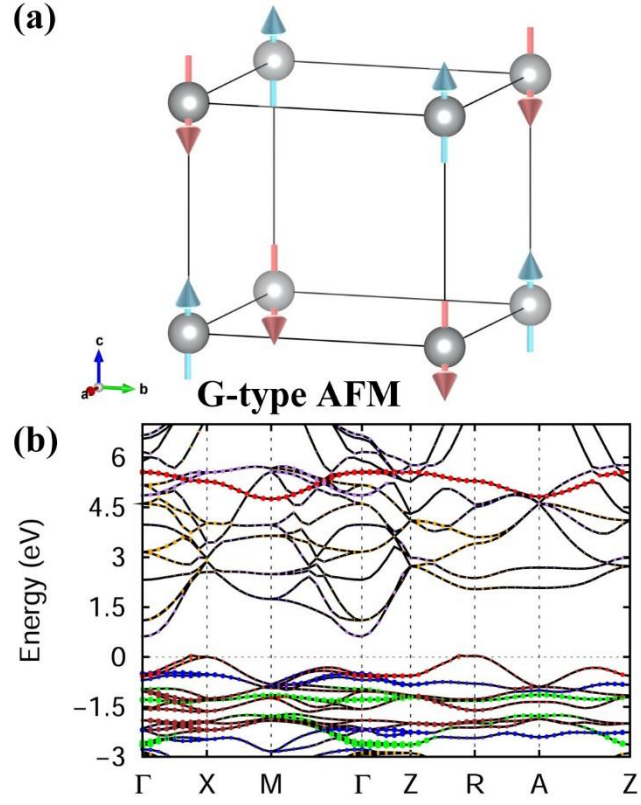


FIG. 9. (a) The G-type of antiferromagnetic (AFM) order. (b) HSE06 band structures of G-type AFM states for a $\sqrt{2} \times \sqrt{2} \times 2$ supercell in the polar BiNiO₂. The color has the same meanings as in Fig. 4.

- [1] K. Rabe, C. H. Ahn, and J.-M. Triscone, *Physics of ferroelectrics: A modern approach* (Springer, Heidelberg, 2007).
- [2] Y. Wang, X. Liu, J. D. Burton, S. S. Jaswal, and E. Y. Tsymlal, Ferroelectric instability under screened Coulomb interactions, *Phys. Rev. Lett.* **109**, 247601 (2012).
- [3] P. W. Anderson and E. I. Blount, Symmetry considerations on martensitic transformations: "Ferroelectric" metals?, *Phys. Rev. Lett.* **14**, 217 (1965).
- [4] Y. Shi *et al.*, A ferroelectric-like structural transition in a metal, *Nat. Mater.* **12**, 1024 (2013).
- [5] W. Cai *et al.*, Pressure-induced ferroelectric-like transition creates a polar metal in defect antiperovskites Hg₃Te₂X₂ (X = Cl, Br), *Nat. Commun.* **12**, 1509 (2021).
- [6] T. H. Kim *et al.*, Polar metals by geometric design, *Nature* **533**, 68 (2016).
- [7] S. Lei *et al.*, Observation of Quasi-Two-Dimensional Polar Domains and Ferroelastic Switching in a Metal, Ca₃Ru₂O₇, *Nano Lett.* **18**, 3088 (2018).
- [8] H. Zhang, B. Deng, W. C. Wang, and X. Q. Shi, Parity-breaking in single-element phases: ferroelectric-like elemental polar metals, *J. Phys.: Condens. Matter.* **30**, 415504 (2018).
- [9] D. Li, K. Lee, B. Y. Wang, M. Osada, S. Crossley, H. R. Lee, Y. Cui, Y. Hikita, and H. Y. Hwang, Superconductivity in an infinite-layer nickelate, *Nature* **572**, 624 (2019).
- [10] R. O. Jones, Density functional theory: Its origins, rise to prominence, and future, *Rev. Mod. Phys.* **87**, 897 (2015).
- [11] J. P. Perdew, K. Burke, and M. Ernzerhof, Generalized Gradient Approximation Made Simple, *Phys. Rev. Lett.* **77**, 3865 (1996).
- [12] G. Kresse and J. Furthmüller, Efficient iterative schemes for ab initio total-energy calculations using a plane-wave basis set, *Phys. Rev. B* **54**, 11169 (1996).
- [13] M. Gajdoš, K. Hummer, G. Kresse, J. Furthmüller, and F. Bechstedt, Linear optical properties in the projector-augmented wave methodology, *Phys. Rev. B* **73** (2006).
- [14] J. Hafner, Ab-initio simulations of materials using VASP: Density-functional theory and beyond, *J Comput Chem* **29**, 2044 (2008).
- [15] J. Heyd, G. E. Scuseria, and M. Ernzerhof, Hybrid functionals based on a screened Coulomb potential, *J. Chem. Phys.* **118**, 8207 (2003).
- [16] H. J. Monkhorst and J. D. Pack, Special points for Brillouin-zone integrations, *Phys. Rev. B* **13**, 5188 (1976).
- [17] R. D. King-Smith and D. Vanderbilt, Theory of polarization of crystalline solids, *Phys. Rev. B* **47**, 1651 (1993).
- [18] A. Togo and I. Tanaka, First principles phonon calculations in materials science, *Scripta Mater.* **108**, 1 (2015).
- [19] A. A. Mostofi, J. R. Yates, Y.-S. Lee, I. Souza, D. Vanderbilt, and N. Marzari, wannier90: A tool for obtaining maximally-localised Wannier functions, *Comput. Phys. Commun.* **178**, 685 (2008).
- [20] A. A. Mostofi, J. R. Yates, G. Pizzi, Y.-S. Lee, I. Souza, D. Vanderbilt, and N. Marzari, An updated version of wannier90: A tool for obtaining maximally-localised Wannier functions, *Comput. Phys. Commun.* **185**, 2309 (2014).
- [21] M. Hepting *et al.*, Electronic structure of the parent compound of superconducting infinite-layer nickelates, *Nat. Mater.* **19**, 381 (2020).
- [22] H. Zhang, L. Jin, S. Wang, B. Xi, X. Shi, F. Ye, and J.-W. Mei, Effective Hamiltonian for nickelate oxides Nd_{1-x}Sr_xNiO₂, *Phys. Rev. Res.* **2**, 013214 (2020).

- [23] A. S. Botana and M. R. Norman, Similarities and Differences between LaNiO₂ and CaCuO₂ and Implications for Superconductivity, *Phys. Rev. X* **10**, 011024 (2020).
- [24] G. W. Watson, S. C. Parker, and G. Kresse, Ab initio calculation of the origin of the distortion of α -PbO, *Phys. Rev. B* **59**, 8481 (1999).
- [25] Y. D. Chong, X.-G. Wen, and M. Soljačić, Effective theory of quadratic degeneracies, *Phys. Rev. B* **77**, 235125 (2008).
- [26] K. Sun, H. Yao, E. Fradkin, and S. A. Kivelson, Topological insulators and nematic phases from spontaneous symmetry breaking in 2D fermi systems with a quadratic band crossing, *Phys. Rev. Lett.* **103**, 046811 (2009).